Int J Fract (2013) 183:105–112
DOI 10.1007/s10704-013-9863-y

LETTERS IN FRACTURE AND MICROMECHANICS

FAILURE OF MAGNESIUM SHEETS UNDER MONOTONIC LOADING: 3D EXAMINATION OF FRACTURE MODE AND MECHANISMS

D. Steglich[a] *, T. F. Morgeneyer*[b]

[a] *Helmholtz-Zentrum Geesthacht Zentrum für Material- und Küstenforschung, Institute of Materials Research, Materials Mechanics, Max-Planck-Str. 1, 21502 Geesthacht, Germany*
[b] *Mines ParisTech, Centre des Matériaux, CNRS UMR 7633, BP87 91003 Evry Cedex, France*

e-mail: dirk.steglich@hzg.de

Abstract. Damage evolution in a commercial magnesium sheet alloy (Mg-3Al-1Zn-0.3Mn) at room temperature is investigated. Kahn tear tests were performed to characterize the crack extension behaviour. Scanning electron microscopy of the fracture surfaces revealed flat inclined areas and the absence of cracked particles and dimples. Post-mortem synchrotron tomography of a stopped crack was used to further identify the predominant damage mechanism in the specimen's ligament. Nucleation of submicrometre-voids, a micro-void sheeting mechanism and the absence of classical void growth could be identified.

Keywords: AZ31, damage mechanism, void sheeting, SEM, tomography.

1. Introduction. Research on magnesium and its alloys has been getting more attention as magnesium is the lightest metal in use for the production of structural components in the automotive and aircraft industry. Despite the high strength-to-weight ratio, the application of wrought magnesium (i.e. sheets and extruded profiles) to light weight structures is limited. Existing applications are mainly based on cast products, whereas the use of sheets for the fabrication of components and structures can still be expanded. The limitation for the structural application of magnesium sheets is correlated with its pronounced anisotropy, the tension-compression asymmetry as well as its comparably poor ductility at room temperature, see (Hosford 1993; Bohlen et al. 2007). While these effects can be explained through the microstructure of the hexagonal-close packed (hcp) material, the mechanisms of material separation might follow different rules. The macroscopic orientation of a propagating crack (failure mode) and failure mechanisms may thereby depend on the loading type and the material orientation. A failure assessment of magnesium structures has to account for the peculiarities related to the microstructure. This will be investigated hereinafter. For this purpose, a common magnesium sheet product was chosen as a testing material.

Numerous investigations address the deformation mechanisms (slip, twinning, de-twinning) in magnesium alloys, but less research is documented towards the mechanisms leading to material separation, in particular for multi-axial stress states. Failure mechanisms of die-cast Mg alloy (AM60B) during tensile loading of smooth specimens have been investigated by Weiler (Weiler et al. 2005). Damage initiation could be seen for pores larger than 80 μm in

diametre. In (Lugo et al. 2011), fracture of coarse (~10 μm in diametre) intermetallic particles has been observed by means of optical microscopy for extruded AZ61 Mg-alloy during tensile loading. Here, we assess a stopped crack in a magnesium alloy that does not contain large particles. Stopped cracks in Kahn specimens (Kahn and Imbembo 1948) made of 2XXX series Al-alloy have been studied in order to investigate the effect of loading direction and stress triaxiality on the failure mode (Morgeneyer and Besson 2011). Differences in void growth behaviour between flat and slant fracture were found. Taking advantage of recent advances in synchrotron laminography, ductile crack progression in flat samples has also been observed in-situ, and in 3D in Al-alloy samples (Morgeneyer et al. 2013; Shen et al. 2013).

This paper studies the failure behaviour of the well-established magnesium sheet alloy AZ31 (nominal composition of 3 wt.% Al, 1 wt.% Zn, 0.3 wt.% Mn, balance Mg) with a thickness of 1 mm under monotonic tensile loading conditions at room temperature using Kahn specimens. The macroscopic quantities recorded during testing are correlated to the failure mode. Fractography and a post-mortem tomography are used to identify the dominant damage mechanism.

2. Microstructure and mechanical tests. The microstructure of the investigated material can be inspected from Figure 1. It shows a fully recrystallised microstructure observed in the plane span by the rolling direction (RD) and the short transverse or normal direction (ND), (RD-ND)-plane. Regions with smaller grains are present in shear bands which developed during rolling. However, the grain size distribution can still be regarded as being homogenous. The average grain size measured in two perpendicular planes collinear with the normal direction (ND) is 5 microns. Precipitates appear as black dots in the figure. Their size appears unrealistically large, as the etchant used caused heavy corrosion.

Nine Kahn specimens (dimensions: 35 mm x 60 mm x 1.0 mm) were machined along three different orientations, namely RD (rolling direction is the main loading direction), TD (transverse direction) and 45° with the rolling direction. Electro-discharge machining (EDM) was used to avoid the mechanical damage associated with conventional machining. The tensile load (displacement control) was applied with a rate of 0.003 mm/s. Cracks were grown to a minimum length of 4 mm in the Kahn tear tests. The tests were stopped before final failure of the coupon. The recorded force-crack mouth opening displacement (CMOD) records of one representative specimen per orientation are shown in Figure 2. The recorded force signal was normalised by the ligament's initial cross-section, A_0=25 mm^2 to allow for comparison with thicker specimens and other materials. All specimens show a sudden decrease of the stress once a crack starts to extend. This point is reached earlier in case of the TD-orientation sample and later in case of RD- and 45°-oriented specimens. Small differences in terms of the stress level prior to crack extension between specimens of different orientation are evident, which is a consequence of the plastic anisotropy (Steglich et al. 2012). The unsteady decrease of the external force indicates that the crack extends in an unstable manner. Fractography using a scanning electron microscope revealed a

macroscopically rough fracture surface. Microscopically, two main features can be observed: A very small amount of ductile crack extension in a dimple-dominated triangle region ahead of the initial crack tip (Figure 3a), and the remaining large region showing flat surfaces (Figure 3b) of a size similar to the grain size. While the triangular section is oriented perpendicular to the main loading direction, the major part of the fracture surface is irregularly tilted by 45° against the sheet's normal direction. As dimples are hardly visible on that part of the fracture surface, it seems that failure is not based on void growth and coalescence here. Thus it is not a typical ductile failure mechanism. The fracture surface bears similar features like the one described recently (Liang et al. 2013), where "quasicleavage fracture characteristics" are reported for a extruded Mg-alloy of similar chemical composition.

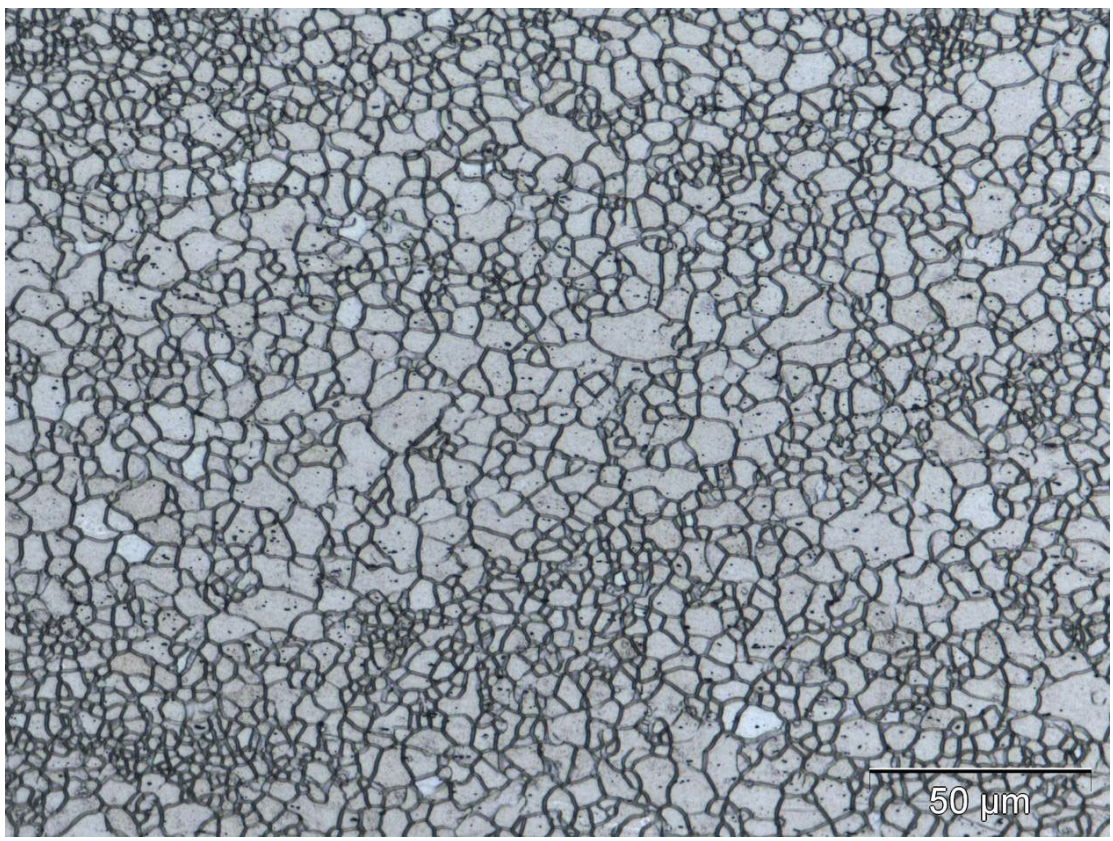

Figure 1: Optical micrograph of a longitudinal section (RD-ND plane) after etching of the AZ31-sheet showing a recrystallised microstructure and precipitates inside the grains.

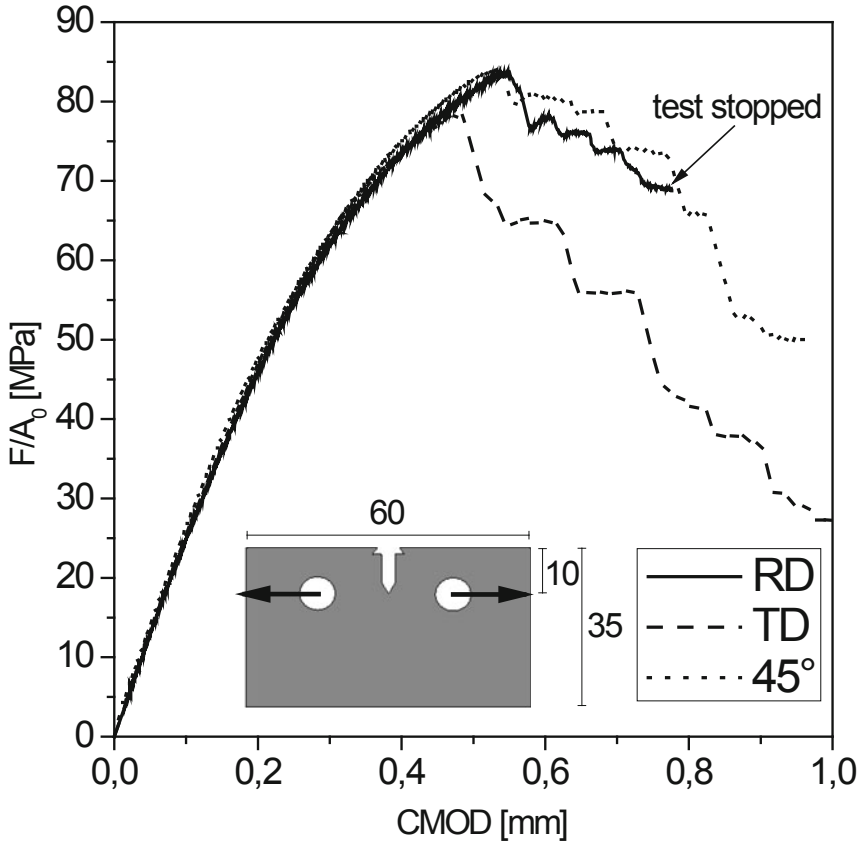

Figure 2: Normalised force-CMOD behaviour of the tested samples. Specimen loaded in RD-orientation was further investigated. Measures in mm.

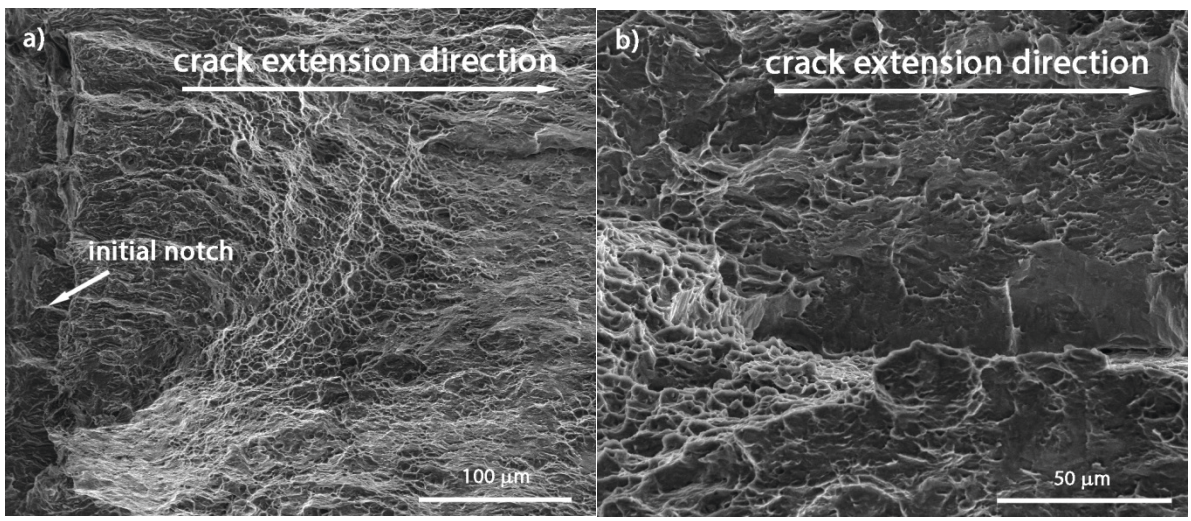

Figure 3: SEM micrographs showing the fracture surface ahead of the initial notch tip with small dimples (a) and in the flat-to-slant transition region showing flat surfaces with micro-dimples (b).

3. 3D-tomography. One sample oriented in RD-direction was chosen for a more detailed investigation of the crack extension in the ligament using 3D-tomography. To facilitate high resolution SRCT imaging of the arrested crack tip region, a small prism of material (dimensions 1.5 mm x 1 mm x 10 mm) was extracted around the tip (long dimension parallel to the direction of crack extension) using EDM. Tomography was performed at beamline ID 19 of the European Synchrotron Radiation Facility (ESRF), Grenoble, France, at 19kV. For one volume 1500 radiographs were taken whilst the sample was turned through 180° (parallel beam conditions). In the reconstructed slices an isotropic voxel size of 0.7 μm was obtained. Phase contrast imaging has been performed to enhance the detection of edges (Kocsis and Snigirev 2004). At ID19 this is a straightforward technique as advantage is taken of the radiation coherence by adjusting the sample-detector distance (~7.5 mm in the present work) to obtain near-field Fresnel diffraction effects. Four scans of about 1 mm3 have been carried out to assess the entire crack via tomography. The four reconstructed 3D images have subsequently been concatenated together using the software ImageJ. The local crack opening displacement was calculated and visualised with an in-house code based on Python and Matlibplot (Morgeneyer et al. 2009).

Figure 4 shows tomography data of the stopped crack in terms of local crack opening displacement (COD) (Figure 4a) and in terms of 2D sections normal to the crack propagation direction at different distances from the notch root (Figure 4b-g). Figure 4a gives an overview over the crack from the notch root to the crack tip. The locations where the 2D sections were taken are indicated. It can be seen that the crack tip is neither straight nor tunnelling but inclined with respect to the specimen surface. The bright regions in the local CTOD map represent the regions near the surface where shear lips separate from each other due to non-symmetric (mode III) opening of the crack. In the middle of the crack at 1 mm from the notch root some uneven local crack tip opening can be seen that is a hint for the surface roughness in this area.

Figure 4b shows a 2D section at the notch root. The curved sides of the specimen result from necking of the ligament. Some opened crack regions can be seen as well as narrow regions and crack bifurcation. However, in contrast to other engineering alloys such as aluminium alloys, no second phase particles are discernible in this AZ31 alloy that could act as void nucleation sites. Around the crack hardly any micrometric voids are visible. Figure 4c shows a region 0.1 mm away from the notch root. Again only very few voids can be seen around the crack (black spots). This is astonishing as the stress triaxiality is expected to be at a maximum in the crack initiation region and a high triaxiality is known to trigger void growth (Bron and Besson 2006). The opened regions of the crack seem to be less caused by void growth but by the crack surface opening, because the opposite surfaces would still fit together. Some white features can be seen at the mid-thickness: Heavy particles, which are however not cracked. Figure 4d is taken at ~0.4 mm from the notch root. No voids are seen around the crack that has a zig-zag shape and a very smooth fracture surface. Again, the damage process does not seem to be consistent with a classical ductile damage process that includes pre-existing voids or void nucleation at brittle particles, their subsequent growth

and coalescence. Despite the expected high levels of stress triaxiality no micrometric voids are seen here either. The damage process consists of strain localisation in very narrow inclined bands followed by sudden failure at sub-micrometre scale. Figure 4e shows the crack at 1.5 mm from the notch root. Near the surface smooth areas corresponding to shear lips are present whereas the centre of the crack is rough. There still seems to be little void growth but the rough surface points to a different fracture mechanism compared to the shear lips. Possibly the increased level of stress triaxiality in the centre of the specimen favours a failure of grain boundaries but supplementary experimental assessments would be necessary to confirm this point. Figure 4f and g represent cross-sections at 2.5 mm and 3.5 mm from the notch root, respectively. Again the competition between smooth shear lip failure and rough surface failure can be inspected. In addition, the "overshoot" of two orthogonal damage planes can be seen in the two images. This seems to indicate that orthogonal strain bands are active during tearing that lead to cracking of the material. In Figure 4g (corresponds to the stopped crack tip) there are hardly any voids ahead of the crack visible. The crack extension mechanism seems to be governed by simultaneous nucleation and coalescence of sub-micrometre voids in the strain bands (see also fractography in Figure 3). Void growth cannot be observed.

4. Conclusons. The underlying damage mechanisms during crack progression in AZ31 alloy at room temperature were investigated via 3D synchrotron tomography of a 4 mm long stopped crack in a 1 mm thick Kahn specimen and via post-mortem fractography. The observed damage mechanisms are different from classical ductile failure. No void growth around the crack is seen and the crack tip itself is very narrow. Smooth shear areas were found close to the specimen's surface as well as hardly opened rough areas in the specimen centre, which is possibly linked to intergranular cracking. At various places the crack formed a 45° zig-zag pattern in through-thickness direction. Heavy particles found at specimen mid-thickness were not fractured. Nano-sized dimples seen on the fracture surface by SEM fractography suggest a sudden nucleation and coalescence of these nano-voids commonly referred to as void-sheeting mechanism.

Modelling activities aiming on the predictions of damage of fracture should consider this finding. Damage models based on evolution laws for void growth like the GTN, Rousselier models and their derivatives (Gurson 1977; Pardoen and Hutchinson 2000; Rousselier 1987) seem not to be an appropriate choice. Macroscopically, failure is not only triggered by the strain, but strongly affected by the triaxiality, see (Steglich et al. 2012). Thus, failure loci span by these two quantities might be promising candidates for modelling purposes. A void nucleation model (Horstemeyer and Gokhale 1999) is shown to capture damage progression caused by fracture of intermetallics in extruded AZ61 on a local level (Lugo et al. 2011), but its application to structures has not been shown yet. Once elevated temperatures are considered, the failure mechanism changes, and consequently the ductility does. Ductile failure of the same alloy is reported and characterised for temperatures of 400°C (Lhuissier et al. 2013). In this regime constitutive equations based accounting for elasto-plasic deformation and void growth (e.g. the one by (Yoon et al. 2011) taking into account the

strength differential effect) possibly can be applied. However, viscous effects should be considered here.

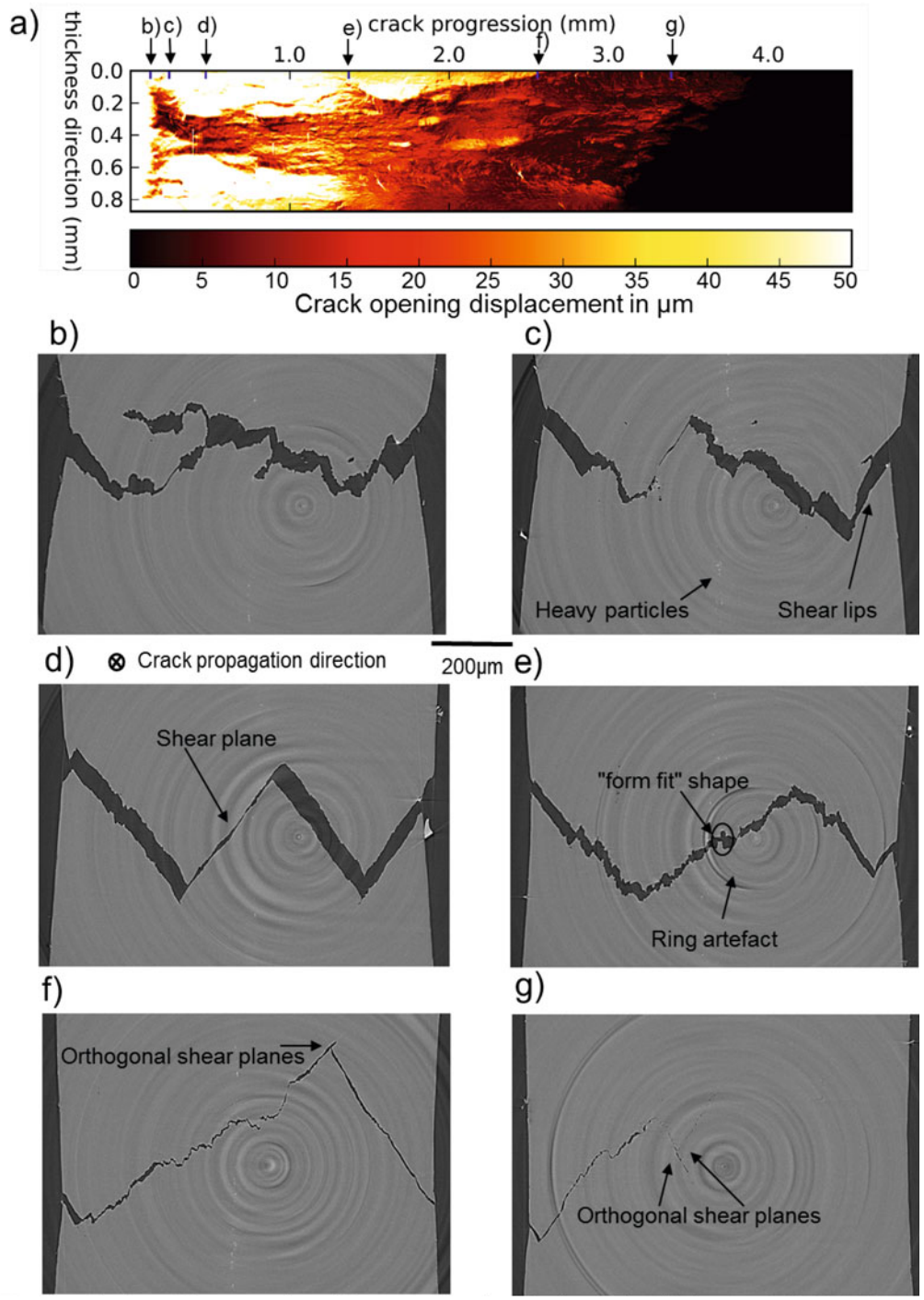

Figure 4: Tomography data of the stopped crack in terms of local crack tip opening displacement (CTOD) (a) and in terms of 2D sections normal to the crack propagation direction at different distances from the notch root (b)-(g).

Acknowledgements. The present work was initiated during an international outgoing fellowship (Marie Curie Actions) of the 7th programme of the European Commission. The authors acknowledge this support and hereby point out that the EU is not responsible for the content of this paper. The authors furthermore thank POSCO (Korea) for providing the sheet material and A. Meddour for his support during mechanical testing. Support from Lukas Helfen at ESRF beamline ID19 for tomography is furthermore acknowledged.

References

Bohlen J, Nuernberg MR, Senn JW, Letzig D, Agnew SR (2007) The texture and anisotropy of magnesium–zinc–rare earth alloy sheets. *Acta Mater* **55**:2101-2112

Bron F, Besson J (2006) Simulation of the ductile tearing for two grades of 2024 aluminum alloy thin sheets. *Eng Fract Mech* **73** (11):1531-1552

Gurson AL (1977) Continuum theory of ductile rupture by void nucleation and growth: Part -1 yield criteria and flow rules for porous ductile media. *Journal of Engineering Materials and Technology*, **99**:2-15

Horstemeyer MF, Gokhale AM (1999) A void-crack nucleation model for ductile metals. *Int J Solids Struct* **36**:5029-5055

Hosford WF (1993) The mechanics of crystals and textured polycrystals. Oxford University Press, New York

Kahn NA, Imbembo EA (1948) A method of evaluating transition from shear to cleavage failure in ship plate and its correlation with large-scale plate tests. *Welding J* **27** (4):169-184

Kocsis M, Snigirev A (2004) Imaging using synchrotron radiation. *Nuclear Instruments & Methods in Physics Research* Section a-Accelerators Spectrometers Detectors and Associated Equipment **525** (1-2):79-84.

Lhuissier P, Scheel M, Salvo L, Di Michiel M, Blandin JJ (2013) Continuous characterization by X-ray microtomography of damage during high-temperature deformation of magnesium alloy. *Scripta Materialia* **69** (1):85-88.

Liang H, Pan F, Wang J, Yang J (2013) Tensile and Compressive Properties of Mg-3Al-2Zn-2Y Alloy at Different Strain Rates. *J of Materi Eng and Perform*:1-10.

Lugo M, Tschopp MA, Jordon JB, Horstemeyer MF (2011) Microstructure and damage evolution during tensile loading in a wrought magnesium alloy. *Scripta Materialia* **64** (9):912-915.

Morgeneyer TF, Besson J (2011) Flat to slant ductile fracture transition: Tomography examination and simulations using shear-controlled void nucleation. *Scripta Materialia* **65** (11):1002-1005.

Morgeneyer TF, Besson J, Proudhon H, Starink MJ, Sinclair I (2009) Experimental and numerical analysis of toughness anisotropy in AA2139 Al-alloy sheet. *Acta Materialia* **57** (13):3902-3915

Morgeneyer TF, Helfen L, Mubarak H, Hild F (2013) 3D Digital Volume Correlation of Synchrotron Radiation Laminography Images of Ductile Crack Initiation: An Initial Feasibility Study. *Experimental Mechanics* **53** (4):543-556.

Pardoen T, Hutchinson JW (2000) An extended model for void growth and coalescence. *J Mech Phys Solids* **48** (12):2467-2512

Rousselier G (1987) Ductile fracture models and their potential in local approach of fracture. *Nucl Eng Des* **105**:97-111

Shen Y, Morgeneyer TF, Garnier J, Allais L, Helfen L, Crépin J (2013) Three-dimensional quantitative in situ study of crack initiation and propagation in AA6061 aluminum alloy sheets via synchrotron laminography and finite-element simulations. *Acta Materialia* **61** (7):2571-2582.

Steglich D, Jeong Y, Andar MO, Kuwabara T (2012) Biaxial deformation behaviour of AZ31 magnesium alloy: Crystal-plasticity-based prediction and experimental validation. *International Journal of Solids and Structures* **49** (25):3551-3561

Weiler JP, Wood JT, Klassen RJ, Maire E, Berkmortel R, Wang G (2005) Relationship between internal porosity and fracture strength of die-cast magnesium AM60B alloy. *Materials Science and Engineering A* **395** (1-2):315-322

Yoon JH, Stewart JB, Cazacu O (2011) Coupled elastic–plastic damage model for a porous aggregate with an incompressible matrix displaying tension–compression asymmetry. *Engineering Fracture Mechanics* **78** (7):1407-1423.